

RESEARCH ARTICLE | OCTOBER 16 2023

# Evaluation of algebraic models of anomalous transport in a multi-fluid Hall thruster code

Thomas A. Marks  ; Benjamin A. Jorns 

 Check for updates

*J. Appl. Phys.* 134, 153301 (2023)

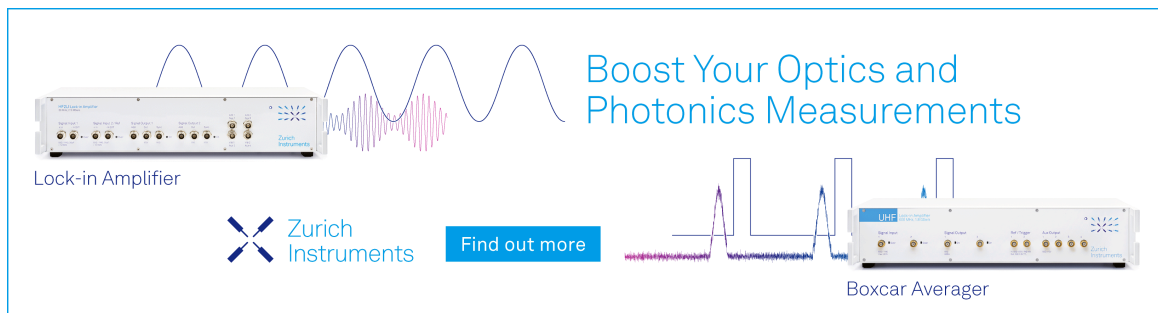
<https://doi.org/10.1063/5.0171824>




CrossMark

22 March 2024 03:08:42

Boost Your Optics and Photonics Measurements



Lock-in Amplifier

 Zurich Instruments

[Find out more](#)

Boxcar Averager

# Evaluation of algebraic models of anomalous transport in a multi-fluid Hall thruster code

Cite as: J. Appl. Phys. 134, 153301 (2023); doi: 10.1063/5.0171824

Submitted: 10 August 2023 · Accepted: 28 September 2023 ·

Published Online: 16 October 2023



Thomas A. Marks<sup>a)</sup>  and Benjamin A. Jorns 

## AFFILIATIONS

Department of Aerospace Engineering, University of Michigan, Ann Arbor, Michigan 48109, USA

<sup>a)</sup> Author to whom correspondence should be addressed: [marksta@umich.edu](mailto:marksta@umich.edu)

## ABSTRACT

The behavior of four algebraic closure models for anomalous electron transport is investigated using a fluid Hall thruster code. The models, which were selected because they have been previously described in the literature, are calibrated against a baseline experimental condition of a 9-kW-class magnetically shielded Hall thruster operating at 300 V and 15 A on xenon propellant. The extensibility of the models is then assessed by using this calibrated model to simulate three additional operating conditions—300 V and 30 A, 600 V and 15 A, and 300 V and 15 A operating on krypton propellant. The quality of the model prediction is quantified by comparing the model outputs to experimental measurements of discharge current, thrust, and ion velocity. It is found that while none of the models can predict the ion acceleration characteristics accurately, some compare favorably in terms of the scaling of thrust and discharge current across operating conditions. The limitations of the models are attributed to the coupling between the functional scaling of the closure models with respect to the local plasma properties and the fluid model. The role of the electron energy balance in this coupling is also highlighted. These results are discussed in the context of motivating improved closure models of the anomalous electron transport in Hall thrusters.

Published under an exclusive license by AIP Publishing. <https://doi.org/10.1063/5.0171824>

## I. INTRODUCTION

Hall thrusters are the most widely flown type of in-space electric propulsion device, with applications ranging from station-keeping and drag compensation to deep space exploration.<sup>1–3</sup> The efficient operation of these crossed-field, low-temperature plasma devices depends on a number of physical processes, some of which remain poorly understood despite decades of research and development.<sup>4</sup> The most consequential of these is the problem of enhanced non-classical electron transport across the thruster's magnetic field lines. This so-called “anomalous” transport governs many aspects of the physics of Hall thrusters and, therefore, the performance of the device. As this transport is not yet fully understood, there has yet to be a fully self-consistent, predictive model of Hall thruster operation. This type of predictive ability is highly desirable as it can inform new thruster designs outside the traditional operating envelope<sup>5</sup> and reduce the ground testing requirements to qualify new thruster designs.<sup>6</sup> It is, therefore, critical to be able to model anomalous electron transport in order to predict how these thrusters operate.

There is growing consensus that this transport can be attributed to the onset of azimuthally directed instabilities that grow at the expense of the electron drift.<sup>4,7–9</sup> This creates azimuthal drag

which, in turn, promotes cross-field transport. A key challenge in capturing this effect, thus, is to develop simulations that can self-consistently represent the growth of the waves of interest. To this end, both fluid and kinetic simulations have been employed.

Recently, fully kinetic three-dimensional particle in cell simulations have enabled detailed studies of this transport.<sup>10</sup> However, such simulations are highly computationally intensive, requiring months of wall time and hundreds to thousands of CPU cores. Scaling these simulations to realistically sized thrusters and operating times has been prohibitively computationally expensive to date. While there is ongoing research to address the technical challenges with developing fully kinetic models that represent thruster operation,<sup>11</sup> a common alternative is to treat the electrons as a fluid.<sup>12</sup>

These simulations are typically less expensive than kinetic simulations, with run times on the order of hours to days. For this reason, fluid models are, thus, widely used for engineering design purposes.<sup>5,13,14</sup> Fluid simulations that resolve the azimuthal dimension have been able to show the onset of instabilities that can also enhance transport,<sup>15,16</sup> but there remains an open question as to whether these are the same modes that drive transport in actual systems. This stems largely from the fact that the modes are

22 March 2024 03:08:42

believed to be kinetically driven. This invites a closure problem of how to analytically represent the complex physics driving anomalous electron transport in a fluid model of a Hall thruster.

To this end, several researchers have proposed models of the anomalous electron transport for fluid simulations of Hall thrusters. These have been informed by assumptions about the underlying physics governing the transport<sup>17–19</sup> or by data-driven methods.<sup>20</sup> However, some of these models have yet to be implemented self-consistently in a Hall thruster simulation. In the cases where models have been incorporated into fluid models, the predictions were shown to deviate from experimental data, and the lack of a parametric comparison across operating conditions invites questions about model extensibility. More broadly, there has not yet been a published comparison of proposed closures on the same thruster with the same fluid model. As a result, differences between transport models cannot be unambiguously shown to result from the anomalous transport models themselves, instead of differences in simulation parameters. In order to advance the state of the art in predictive engineering simulations of Hall thrusters, there is, thus, a need to systematically evaluate proposed transport closure models with a common fluid model and to compare their predictions to experimental data.

This paper is organized in the following way. In Sec. II, we review the problem of anomalous transport in Hall thrusters. Then, in Sec. III, we describe the four closure models evaluated in this work. In Sec. IV, we describe our model calibration and simulation procedure, our chosen fluid code, and the experimental data to which the model predictions are compared. In Sec. V, we present our results, and in Sec. VI, we interpret these results in the context of the physics of Hall thruster operation and future modeling attempts. Lastly, in Sec. VII, we summarize our findings.

## II. THE PROBLEM OF ANOMALOUS ELECTRON TRANSPORT IN HALL THRUSTERS

In this section, we overview Hall thruster operation, the problem of anomalous transport, and how anomalous transport can be represented in a fluid framework.

### A. Hall thruster operation

A Hall thruster (Fig. 1) is a crossed-field plasma device consisting of a ring-shaped discharge channel, a conductive anode, a hollow cathode, and a magnetic circuit. A voltage,  $V_d$ , is applied between the anode and the cathode, giving rise to an axial electric field,  $\vec{E}$ . The device's magnetic circuit produces a radial magnetic field,  $\vec{B}$ , perpendicular to the applied electric field. Electrons (denoted  $\ominus$  in the diagram) are emitted from the cathode and move against the electric field into the channel. The influence of the crossed electric and magnetic fields in the thruster causes the electrons to drift azimuthally around the device, perpendicular to both electric and magnetic fields. This gives rise to a Hall current,  $\vec{j}_{de}$ , from which the device derives its name.

Simultaneously, neutral atoms ( $\odot$ ), typically xenon or krypton, are injected near the anode. Electrons trapped in the Hall drift impact these atoms with sufficient energy to strip off one or more of the electrons in the atoms' outer valence shell. The atom is, thus, ionized, and the lost electron joins the drift. The magnetic field

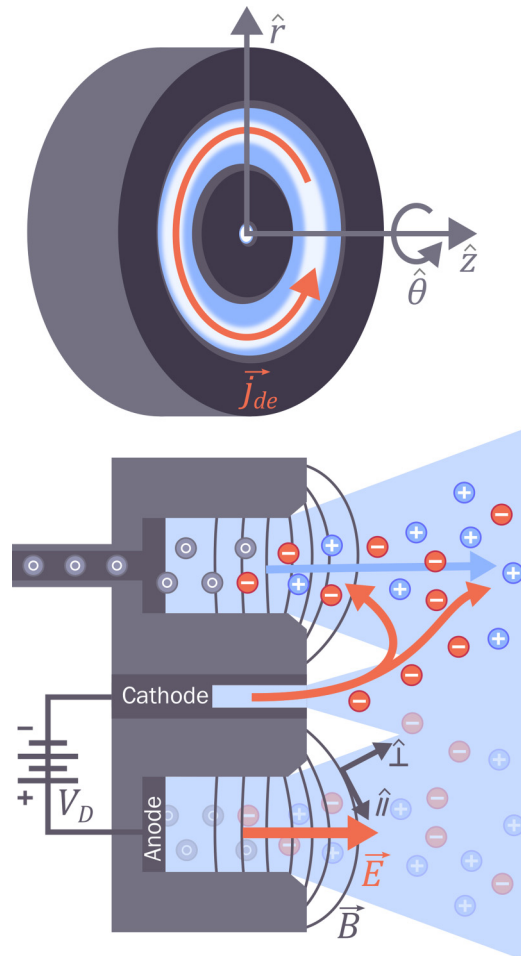


FIG. 1. Operating principle of a Hall thruster, showing major drifts and axisymmetric Cartesian and field-aligned coordinate systems.

strength in the channel is tailored in such a way that the ions resulting from ionization (labeled  $\oplus$  in the diagram) are unmagnetized. The influence of the magnetic field is, thus, negligible, and the ions are accelerated rapidly downstream by the electric field, producing thrust. Additional electrons from the cathode join the departing ions so that the device remains electrically neutral overall.

### B. Anomalous electron transport

It is a standard approximation in fluid models for low-temperature plasma devices ( $T_e < 100$  eV) like Hall thrusters to represent the electron dynamics with a drift-diffusion equation given by the generalized Ohm's law,

$$q_e n_e \vec{E} - \vec{j}_e \times \vec{B} + \nabla p_e + \vec{R}_e = 0. \quad (1)$$

In this expression,  $q_e$  is the fundamental charge,  $n_e$  is the electron number density,  $\vec{E}$  is the electric field vector,  $\vec{j}_e$  is the electron

22 March 2024 03:08:42

current density vector,  $\vec{B}$  is the magnetic field vector,  $p_e$  is the electron pressure, and  $\vec{R}_e$  is the forcing term on the electrons. This equation can be derived by neglecting the inertial terms in the electron fluid momentum equation. Classically, the forcing term can be represented as a collisional drag term between the electrons and other species, such as ions and neutral atoms,

$$\vec{R}_e = -\frac{m_e}{q_e} \vec{j}_e \nu_e, \quad (2)$$

where  $\nu_e$  is the total effective momentum transfer collision frequency between electrons and these heavier species.

In order for the circuit to be complete in the Hall thruster, some electrons must deviate from the Hall drift, cross the magnetic field lines, and reach the anode. This cross-field current can be inferred by combining Eqs. (1) and (2) as

$$j_{e\perp} = \frac{\sigma_e}{1 + \Omega_e^2} (q_e n_e E_{\perp} + \nabla p_e). \quad (3)$$

Here, the  $\parallel$ ,  $\perp$ , and  $\theta$  subscripts denote vector components in the field-parallel, field-perpendicular, and azimuthal directions, respectively.  $\sigma_e = q_e^2 n_e / m_e \nu_e$  is the classical electron electrical conductivity, and  $\Omega_e = \omega_{ce} / \nu_e$  is the classical electron Hall parameter defined as the ratio between the cyclotron frequency,  $\omega_{ce}$ , and classical collision frequency. When the electrons are strongly magnetized ( $\Omega_e \gg 1$ ), which is the case in most regions of the Hall thruster discharge, this equation reduces to

$$j_{e\perp} = \frac{q_e}{m_e} \frac{\nu_e}{\omega_{ce} B} (q_e n_e E_{\perp} + \nabla p_e). \quad (4)$$

This equation shows that collisions between the electrons and heavier species (neutrals and ions) allow the electrons to drift toward the anode. However, it has been shown experimentally that the measured cross-field electron current in Hall thrusters is orders of magnitude larger than can be explained by the electric field, pressure gradients, and classical collision frequency.<sup>4</sup>

Faced with this limitation, it is common in fluid simulations of Hall thrusters to introduce an ‘‘anomalous’’ drag force to promote additional cross-field electron transport. The effective drag on electrons is, thus, modified to

$$\vec{R}_e = -\frac{m_e}{q_e} \vec{j}_e (\nu_e + \nu_{an}), \quad (5)$$

where we have introduced an a transport coefficient,  $\nu_{an}$  that is often interpreted as an ‘‘anomalous collision frequency.’’ This term is typically assumed to be much larger than the classical collision frequency. Armed with this assumption, the equation for cross-field transport now becomes

$$j_{e\perp} = \frac{q_e}{m_e} \frac{(\nu_e + \nu_{an})}{\omega_{ce} B} (q_e n_e E_{\perp} + \nabla p_e). \quad (6)$$

Physically, by adjusting the magnitude of the anomalous collision frequency, it is possible to re-create the magnitude of cross-field transport observed in the experiment. In practice, however, understanding the nature of this effective transport coefficient poses a major challenge for self-consistent fluid modeling.

### III. CLOSURE MODELS FOR THE ANOMALOUS COLLISION FREQUENCY

Introducing  $\nu_{an}$  creates a *problem of closure* in the fluid equations, meaning that we have one more variable than we have equations. Indeed, while the classical expression for  $\nu_e$  can be related from first-principles to conventional fluid properties, a similar form for the anomalous collision frequency is not known. To resolve this, we need to close the system of governing equations by introducing an expression that either explicitly or implicitly determines  $\nu_{an}$  in terms of the other fluid properties.

In keeping with the nomenclature and extensive body of work applying to classical fluid modeling,<sup>21</sup> the nature of closure models for transport in Hall thruster is defined based on the number of differential equations that are employed. *Algebraic* or *zero-equation* models are approaches in which the anomalous collision frequency is given as an explicit function of other plasma properties. This is in contrast to *multi-equation* models, in which one or more partial differential transport equations would need to be solved in order to determine the anomalous collision frequency.<sup>22,23</sup> Algebraic models ultimately are easier to implement and evaluate than multi-equation closures and are more common in the literature.<sup>18–20,24</sup> Indeed, there have been many attempts at algebraic closure for Hall thruster transport to date. Previous investigators have used *ad hoc* empirical models, introducing parameters which must be tuned for each device.<sup>25,26</sup> Others have derived first-principles models, invoking assumptions about the nature and scaling of the kinetic effects that give rise to the anomalous transport.<sup>18,19</sup>

We focus in this work on four previously published attempts at algebraic closure, which we described in Sec. III B. Before reviewing these, however, we first overview our current, experimentally informed understanding of how transport should vary in the thruster. We use this as a reference case in our subsequent discussion.

#### A. Empirically inferred reference case for electron transport

Nearly three decades of Hall thruster simulation research and experiment have shown that the anomalous collision frequency in Hall thrusters is spatially non-uniform. In the absence of a predictive closure model, the anomalous collision frequency must, thus, be tuned as a function of space in order for simulations to match the experiment.<sup>25,27</sup> The empirical anomalous collision frequency profile thus obtained is often treated as a surrogate ‘‘measurement’’ of the anomalous collision frequency in the device. Typically, these empirical profiles follow a Bohm-like transport scaling, in which the anomalous collision frequency is proportional to the electron cyclotron frequency, i.e.,  $\nu_{an}(z) = \alpha(z)\omega_{ce}(z)$ . The constant of proportionality,  $\alpha(z)$ , is a spatially varying proportionality factor between the anomalous and cyclotron frequencies. This factor can be tuned to match data from a given thruster and operating condition.

As a representative example, in Fig. 2(a), we show one such empirically derived profile, obtained for the H9, 9-kW class Hall thruster, along the channel centerline. The thruster and operating condition we used to generate these illustrative results is described in more detail in Sec. IV A. We also show in this plot the cyclotron

22 March 2024 03:08:42

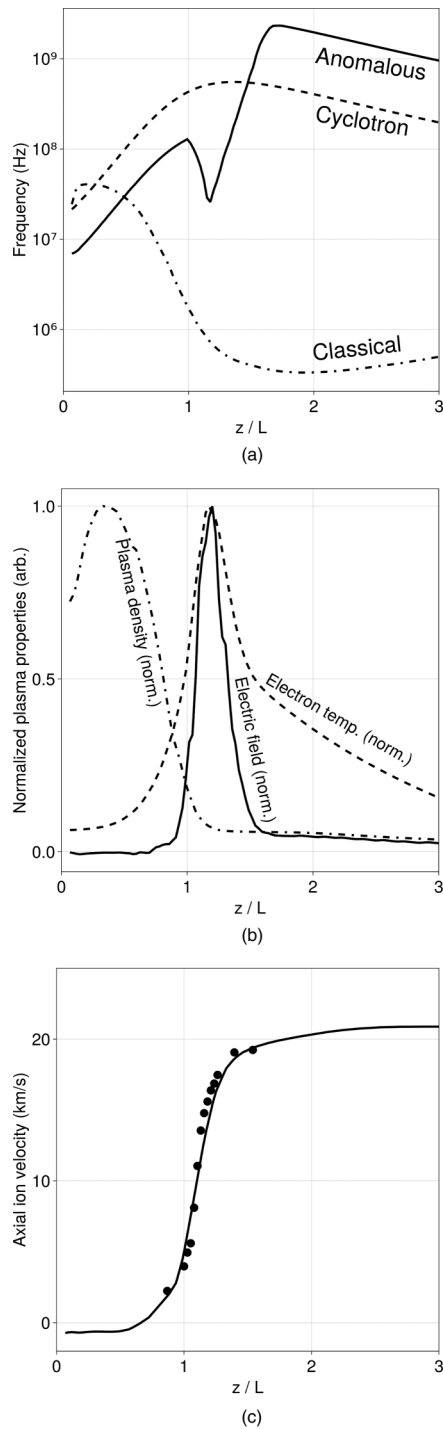


**FIG. 2.** Axial variation of (a) collision frequencies, (b) plasma properties, and (c) ion velocity found in calibrated Hall thruster simulation. Experimental ion velocities measured via laser-induced fluorescence are displayed as markers in (c). Reproduced with permission from Thomas A. Marks and Benjamin A. Jorns, *Plasma Sources Sci. Technol.* **32**, 045016 (2023). Copyright 2023 The Authors.

frequency and classical collision frequency. For comparison, we also include the electron temperature and electric field [Fig. 2(b)], as well as the axial ion velocity [Fig. 2(c)] obtained from a simulation using the empirical profile. In these plots, the distance is referenced with respect to the anode and normalized by channel length. The peak magnetic field occurs at  $z/L \approx 1.2$ , where  $L$  is the length of the discharge channel. In our subsequent discussion, we use empirical profiles like these, which have been calibrated directly against experimental data, as a benchmark for comparison. More qualitatively, we use the following key features exhibited by these profiles as metrics for what we would expect for a successful closure model.

**Minimum coincident with peak magnetic field:** Despite the fact that the anomalous collision frequency dominates the classical collision frequency in most regions of the discharge, the most important feature that a closure model must reproduce is the low anomalous collision frequency near the location of peak magnetic field strength. By Eq. (6), this creates a strong electric field centered at this location, shown in Fig. 2(b). Since electron heating scales as  $\vec{j}_e \cdot \vec{E}$ ,<sup>28</sup> the peak in electron temperature coincides with the peak electric field. The sharply peaked electric field produces rapid ion acceleration, which is required in order to match the steep experimentally observed ion velocity profile indicated markers in Fig. 2(c). This minimum, which serves as a transport barrier for electrons seeking to move upstream, has been observed experimentally and computationally in many thrusters and operating conditions.<sup>17,24,29,30</sup>

**High anomalous collision frequency in near-plume:** Downstream of the minimum, the anomalous collision frequency approaches values on the order of one-tenth to one times the electron cyclotron frequency  $f_{ce} = q_e |\vec{B}| / 2\pi m_e$  and then declines gradually. Upstream of the minimum, the collision frequency may remain low or can be an order of magnitude larger than the value at the minimum, as shown in Fig. 2(a).

With these salient features in mind, we now turn to describing the self-consistent closure models that we will evaluate in this work.

## B. Investigated closure models

We list in summary form in Table I the four closure models we investigated in this work. These four were selected because they have been shown in a select series of cases to yield qualitative agreement with experimental measurements. Practically, each of these models also has only one or two tunable coefficients. This simplifies the process of optimizing each model to find the best agreement with the experiment.

The first model we investigate [Eq. (7)] is from Cappelli *et al.*,<sup>18</sup> who derived a model for the anomalous collision frequency by analogy to classical turbulence theory. We also introduce  $c_e = \sqrt{8T_e/\pi m_e}$ , the electron thermal speed, and a scaling coefficient,  $c_1$ , which is assumed to be constant with respect to other plasma properties and dimensionless. In this model, it is assumed there is plasma turbulence present in the thruster channel. Electrostatic energy enters the turbulent spectrum via the azimuthal Hall drift and then cascades via wave-wave interactions to small scales, where it is dissipated into thermal energy by scattering

22 March 2024 03:08:42

**TABLE I.** Summary of anomalous transport models investigated in this paper.

Model	Expression for $v_{an}$	Eq. No.	Typical coefficients	Proposed mechanism
Cappelli <i>et al.</i>	$v_{an} = c_1 \omega_{ce} \sqrt{\frac{ \vec{j}_{e\perp} E_{\perp} }{q_e n_e c_e^2 B}}$	(7)	$c_1 = 1/\sqrt{2.5} (\approx 0.632)$	Turbulent viscosity (energy cascade)
Lafleur, Balruud, and Chabert	$v_{an} = c_1 \frac{ \nabla \cdot (\vec{u}_i n_e T_e) }{m_e c_s n_e v_{de}}$	(8)	$c_1 = 1/4\sqrt{6} (\approx 0.102)$	EDI saturated by ion-wave trapping
Chodura	$v_{an} = c_1 \omega_{pi} \left[ 1 - \exp\left(-\frac{1}{c_2} \frac{v_{de}}{c_s}\right) \right]$	(9)	$c_1 = 1, c_2 = 3$	Micro-instabilities
Data-driven	$v_{an} = c_1 \omega_{ce} \left( \frac{ \vec{u}_i }{c_2 c_s + v_{de}} \right)$	(10)	$c_1 = 2.39, c_2 = 3.32$	None

electrons. This scattering enhances transport in the same way as classical collisions and, therefore, produces an “anomalous” collisionality. In the paper first describing this model, Cappelli *et al.* compared the results of a 2D axisymmetric hybrid particle-in-cell (hybrid-PIC) simulation carried out using their model to experimental data from Stanford’s Z-70 Hall thruster. They find that the model correctly captures the decrease in mobility near the exit plane (Sec. III A) and produces simulations with velocity profiles similar to those found experimentally via laser-induced fluorescence. However, the researchers did not compare the predicted performance of the simulation to experimental performance measurements in that work.<sup>18</sup>

The second model [Eq. (8)] comes from Lafleur *et al.*<sup>19</sup> In this expression,  $v_{de} = |\vec{E}|/|\vec{B}|$  is the electron drift speed in the azimuthal direction,  $c_s = \sqrt{T_e/m_i}$  is the ion sound speed, and  $\vec{u}_i$  is the velocity vector of singly charged ions. This model was derived based on the assumption that the transport can be attributed to the azimuthal electron drift instability (EDI). This mode has been shown to exist in Hall thrusters and has been experimentally linked to an increase in the effective electron collision frequency.<sup>9,31–34</sup> Physically, in this model, it is assumed that the instability saturates due to ion-wave trapping and convects downstream with the ions. The wave draws its energy from the azimuthal electron drift, so its effect on the fluid equations is that of an effective azimuthal ion-electron drag force which, by the argument in Sec. II, enhances axial electron mobility.

In Ref. 19, this model was shown to be able to replicate—within a scaling factor—empirically derived anomalous electron mobility profiles along the thruster centerline. This included the ability to predict a transport minimum coincident with the location peak magnetic field and high collision frequency both upstream and downstream of this location (Sec. III A). When incorporated

self-consistently into a Hall thruster model for a single operating condition,<sup>35</sup> however, this model predicted lower performance than experiment and an ion acceleration region shifted downstream compared to the experimental results. The extensibility and scaling behavior of this model at other operating conditions has not yet been assessed.

The third model we investigate [Eq. (9)] is based on the formulation of Chodura.<sup>36,37</sup> In this expression,  $\omega_{pi} = \sqrt{q_e^2 n_e / m_i \epsilon_0}$  is the ion plasma frequency and  $\epsilon_0$  is the permittivity of free space. This semi-empirical model describes the effect of microturbulence in a few select types of plasma devices, such as theta-pinch and field-reversed-configuration devices.<sup>38–40</sup> More recently, Simmonds *et al.*<sup>41</sup> proposed that a Chodura-like transport model might apply to Hall thrusters. They investigated the effect of such a scaling on the theoretical thrust density limit for Hall thrusters. However, the model has not yet been implemented self-consistently in a Hall thruster code.

The final model we examine [Eq. (10)] is not derived from first-principles but comes instead from data-driven symbolic regression. In 2018, Jorns<sup>20</sup> used semi-empirical hand-tuned anomalous collision frequency profiles from several thrusters and operating conditions combined with validated simulation data to infer functional forms for the anomalous collision frequency. The result was a series of models which, when computed on time-averaged simulation data, matched the empirical profiles better than investigated first-principles models. These data-driven models could even predict the shape of a profile from a thruster not in the training dataset, including the minimum downstream of the thruster exit plane (Sec. III A). When incorporated self-consistently into a 2D axisymmetric fluid Hall thruster code, one of these models under-predicted thrust by about 20% and over-predicted discharge current by 20%, leading to efficiencies about half of the

experimental values. Additionally, the ion velocity profiles predicted by the model were far more relaxed than those observed experimentally. However, as with the previous closure models, the extensibility of this model has not been fully explored. Similarly, the model calibration procedure employed in the previous work was not as rigorous as the one employed in the present study.

With these models described, we turn in Sec. IV to describing the methods employed in this study.

#### IV. METHODS

In this section, we first introduce the thruster and operating conditions simulated and the data to which we compare our simulation results. We then describe Hall2De, the multi-fluid code we use for all of our simulations. Next, we quantitatively define the metrics by which we compare our simulation results to the data. Finally, we overview our model calibration procedure.

##### A. Thruster and operating conditions

For this work, we simulate the H9 Hall effect thruster, depicted operating at a discharge voltage of 300 V and a discharge current of 15 A using xenon propellant in Fig. 3. This is a 9-kW class magnetically shielded Hall thruster developed in a collaboration between the Air Force Research Laboratory, the Jet Propulsion Laboratory, and the University of Michigan.<sup>42,43</sup> We compare our simulation results to data obtained in two 2021 test campaigns by

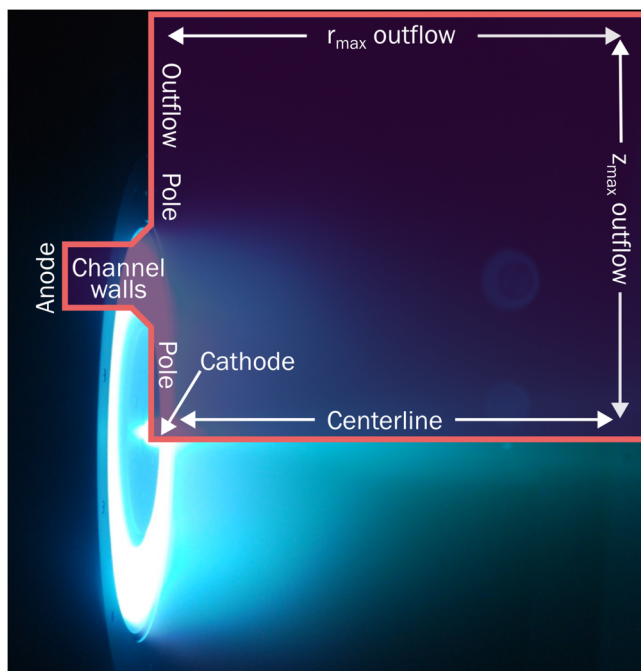


**FIG. 3.** H9 Hall thruster running on xenon at 300 V discharge voltage and 15 A discharge current. Axisymmetric simulation domain (not to scale) is depicted in orange, and boundary surfaces are labeled.

**TABLE II.** H9 operating conditions simulated in this work.

Case No.	$V_D$ (V)	$I_D$ (A)	Propellant	$\dot{m}$ (mg/s)	$P_B$ ( $\mu$ Torr)	$T$ (mN)
1	300	15	Xe	14.8	4.6	$292.9 \pm 3.5$
2	300	30	Xe	26.0	7.6	$539.0 \pm 4.0$
3	600	15	Xe	15.4	5.4	$447.2 \pm 3.0$
4	300	15	Kr	11.8	4.6	$235.8 \pm 2.5$

Su and Jorns.<sup>44,45</sup> These data include performance figures such as thrust and discharge current, as well as spatially resolved ion velocity measurements obtained via laser-induced fluorescence. To investigate how well the models examined in this work can generalize across operating conditions, we consider the subset of operating conditions from Refs. 44 and 45 summarized in Table II. In addition to the nominal 4.5 kW operating condition, where the discharge voltage ( $V_D$ ) was 300 V, the discharge current ( $I_D$ ) was 15 A, and the propellant was xenon, we also simulate high-voltage (600 V and 15 A), high-current (300 V and 30 A), and krypton (300 V and 15 A) cases. For each of the cases, we include the mass flow rate ( $\dot{m}$ ) and background pressure ( $P_B$ ) in the facility, which are needed as simulation inputs, as well as the measured thrust ( $T$ ), to which we compare our simulation results.

##### B. Simulation details

All simulations in this work were conducted using Hall2De, a multi-fluid/particle-in-cell thruster code developed at the Jet Propulsion Laboratory. In this work, we use only the multi-fluid version of the code, the mechanics and solution procedure of which are described in depth in the original paper by Mikellides and Katz.<sup>12</sup> In brief, Hall2De treats both electrons and ions as fluids, while neutrals are treated as a free molecular flow with a line-of-sight view factor algorithm. Multiple ion species are supported, including both higher charge states (up to triply charged), and up to four populations which are distinguished by the electrostatic potential at their origin. In this work, we solved continuity, momentum, and energy equations for each included ion population. The fluid electrons are inertia-less and were, thus, solved using a generalized Ohm's law formulation as outlined in Sec. II. An electron energy equation was also solved.

We summarize the numerical parameters employed for our simulations in Table III. As electrons are strongly magnetized in Hall thrusters, Hall2De solves for their behavior using a mesh aligned with the applied magnetic field. This magnetic field-aligned mesh (MFAM) reduces numerical diffusion and preserves the largely equipotential and isothermal nature of the magnetic field lines while still solving two-dimensional electron energy equations. However, such field-aligned meshes inherently have small, high-aspect-ratio, and high-skewness cells near boundaries and in regions where the magnetic field is convergent. Small time steps are, thus, required to accurately and stably solve the governing equations in these regions. In order to increase the allowable time step and improve numerical stability, we solved the equations of motion for the unmagnetized ions and neutrals on a rectilinear

22 March 2024 03:08:42

TABLE III. Numerical parameters employed in this work.

Maximum charge state	3+
Number of fluids	2 (beam and cathode)
Number of cells (MFAM)	3925
Number of cells (rectilinear grid)	3955
Time step	15 ns
Simulation duration	2 ms
Cathode flow fraction	7%
Cathode ionization fraction	5%
Cathode electron temperature	3 eV
Neutral temperature	500 K
Wall temperature	500 K

grid with more uniform cell sizes. Similar approaches have previously been applied to hybrid-PIC Hall thruster simulations.<sup>46,47</sup>

We employed a MFAM with 3925 cells for the electrons and a rectilinear grid with 3955 cells for the ions. The resolution of each of these grids was selected following a grid convergence study described in Ref. 35. Figure 3 depicts the domain of the simulation with labeled boundaries. The domain extended eight channel lengths downstream from the thruster anode and the same distance radially outward from the channel centerline.

For this work, we simulated three ion charge states and two ion populations. The first ion population comprised ions originating in the main beam, and the second consisted of ions emitted from the cathode or born in the cathode plume. This yielded a total of six ion species. Consistent with the experimental operating conditions described in Sec. IV A, we set the cathode flow rate to be 7% of the anode flow rate. The cathode electron temperature and ionization fraction were then fixed at 3 eV and 5% respectively, which are in line with standalone experimental measurements of the H9 cathode.<sup>48</sup> We fixed both the neutral gas temperature and wall temperature to 500 K.

All of the anomalous transport models described in Sec. III B were implemented using under-relaxation such that the anomalous collision frequency at time step  $n$  was given by a weighted average of the instantaneously computed value and the value computed at time step  $n - 1$ . This improved stability and reduced iteration-to-iteration numerical oscillations, at the cost of a potential reduction in time-accuracy. Since we were primarily interested in time-averaged simulation properties, we considered this an acceptable compromise in favor of improved numerical convergence.

As Hall thrusters are inherently oscillatory devices,<sup>4</sup> our simulations did not converge to a steady state. Instead, after an initial transient, we have found the simulated discharge current will eventually exhibit a quasi-periodic oscillation with constant frequency and amplitude (Fig. 4), with no change in the time-averaged properties. We ran each of our simulations for two milliseconds of simulated time, which was sufficiently long for the simulation to converge to this quasi-stationary state in all cases. With the above numerical parameters, this required around 14 h of wall time per simulation, using a single node with eight CPU cores on the University of Michigan's Great Lakes super-computing cluster.

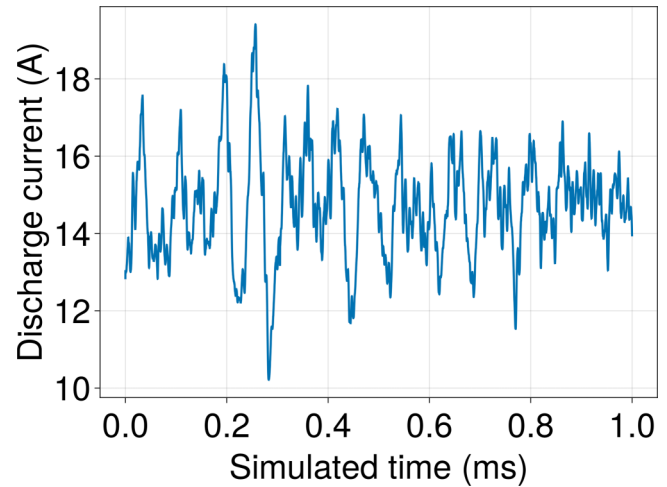


FIG. 4. Example of a converged discharge current trace for a simulation at 300 V and 15 A.

### C. Metrics for comparison to experiment

In order to calibrate and evaluate our simulations, we computed key performance metrics from the simulation output. The first of these was the simulation discharge current ( $I_{D,sim}$ ), which we determined by integrating the current density over the anode boundary surface

$$I_{D,sim} = \iint_{\text{anode}} \left[ \left( \sum_{f=1}^2 \sum_{j=1}^3 j q_e n_{i,f,j} \vec{u}_{i,f,j} \right) + \vec{j}_e \right] \cdot \hat{n} dS. \quad (11)$$

As described in Sec. IV D, we tuned the coefficients of each model so that our simulations matched the experimental discharge current to within 0.5 A, thus ensuring that simulation and experimental current were always the same to within experimental error.

The second metric we evaluated was the simulated thrust,  $T_{sim}$ , which we determined by integrating the flux of axial momentum over the simulation outflow boundaries,

$$T_{sim} = \iint_{\text{outflow}} \sum_{f=1}^2 \sum_{j=0}^3 M n_{f,j} u_{z,f,j} (\vec{u}_{f,j} \cdot \hat{n}) dS. \quad (12)$$

Here,  $\vec{u}_{f,j}$  is the velocity vector of the fluid with index  $f$  and charge  $j$ ,  $u_{z,f,j}$  is the axial component of that vector,  $n_{f,j}$  is the number density of the same fluid, and  $M$  is the mass of the propellant atom. We defined the normalized residual in thrust between simulation and experiment was

$$\text{Thrust residual} = |T_{exp} - T_{sim}| / T_{exp}, \quad (13)$$

where  $T_{exp}$  is the experimental thrust for the current operating condition as reported in Table II.

The third metric we evaluated was the *integrated velocity residual* (IVR), which quantifies how close the simulated ion velocity

22 March 2024 03:08:42



profile is to the experimental profile measured by LIF. We defined the normalized IVR as

$$IVR = \sqrt{\frac{\int_{z_0}^{z_N} (u_{i,LIF}(z) - u_{i,sim}(z))^2 dz}{\int_{z_0}^{z_N} u_{i,LIF}^2(z) dz}}. \quad (14)$$

As an example, this quantity is defined such that if the ion velocity differs from the experimental value by 10% over the axial extent of the data, then the IVR will be 0.1. As a global metric for the validity of the experiment, we combined both normalized residuals to yield

$$\text{Total residual} = IVR + \text{Thrust residual}. \quad (15)$$

Physically, this represents how close a given simulation is to the experimental data, with lower numbers indicating a closer match. It allows for a direct comparison across closure models.

## D. Model calibration and validation

### 1. Empirically derived reference profiles

As discussed in Sec. III A, models of anomalous transport are typically benchmarked against calibrated reference anomalous transport profiles. In order to assess how well the investigated closure models predict the spatial variation of plasma properties, we generated a multi-zone Bohm<sup>26</sup>-like profile for each of the four operating conditions described in Sec. IV A. These profiles were characterized by four “nodes,” ( $z_i, \alpha_i$ ), with the anomalous collision frequency varying logarithmically between these nodes. Specifically, the anomalous collision frequency was given by

$$\frac{v_{an}}{\omega_{ce}} = \begin{cases} \alpha_1 & z < z_1, \\ \exp\left[\log(\alpha_i) + (z - z_i) \frac{\log(\alpha_{i+1}) - \log(\alpha_i)}{z_{i+1} - z_i}\right] & z_i < z \leq z_{i+1}, \\ \alpha_4 & z \geq z_4. \end{cases} \quad (16)$$

To obtain the final profiles, we iteratively adjusted the values of  $z_i$  and  $\alpha_i$  until the simulated ion velocity profiles matched LIF data (IVR  $\leq 0.1$ ) and the thrust residual was less than 10%. In doing so, we obtained a “ground truth” for how plasma properties such as the anomalous collision frequency and electron temperature varied as a function of axial distance from the anode.

### 2. Closure model coefficients

As outlined in Table I, all the investigated closure models have either one or two coefficients. For single-coefficient models [Eqs. (8) and (7)], we adjusted  $c_1$  in order to match the experimental discharge current. For the two-coefficient [Eqs. (9) and (10)] models, we first performed a parameter sweep over  $c_2$ . For each value of  $c_2$ , we then varied  $c_1$  until the experimental discharge current matched within  $\pm 0.5$  A. In each model,  $c_1$  serves to scale the magnitude of the anomalous collision frequency. In turn, we found that the discharge current depended monotonically on  $c_1$ , so that for each  $c_2$ , there was a unique value of  $c_1$  which produced the experimental discharge current. With this complete, we then selected the combination of  $c_1$  and  $c_2$  which minimized the total residual [Eq. (15)].

In both cases, we accelerated the calibration of  $c_1$  using a PID control system integrated into Hall2De. This loop updated every time step and used the figure of merit of the average discharge current inferred from a preceding time window of 400  $\mu$ s. The PID loop constants were tuned using our open-source one-dimensional fluid Hall thruster code HallThruster.jl<sup>49</sup> and subsequently tested in Hall2De. Numerical experiments have shown that the PID loop constants thus obtained are able to effectively control the average discharge current while not damping out strong breathing mode oscillations.<sup>50</sup>

We only applied this calibration procedure for each closure model to one condition, the 300 V, 15 A operating point. Once we obtained values of  $c_1$  and  $c_2$  for each model on this condition, we evaluated the extensibility of each model by simulating the other three operating conditions (Sec. IV A) using these coefficients. With this approach in mind, we now turn to presenting the results of our study.

## V. RESULTS

In Table IV, we report the best-fit values of  $c_1$  and  $c_2$  for all four models, as obtained by the calibration procedure discussed in Sec. IV. We compare these values to results from the best-fit parameters given in previous works. Notably, our coefficients differ by at least a factor of two in each case from the values reported in the literature. This indicates that coefficients inferred for these models may not be extensible across different thrusters and operating conditions.

In Table V, we present the discharge current predicted by each of the models at the four investigated operating conditions using the coefficients displayed in Table IV. We see that for the calibration case (case 1, 300 V and 15 A on xenon), the obtained discharge currents are within 0.2 A of the target value of 15 A. This indicates that the PID controller was able to successfully tune the fit coefficients to match the experimental discharge current. In case 2 (300 V and 30 A on xenon), all four of the models correctly predict that increasing the mass flow rate will increase the discharge current but underestimate the predicted increase by between 2 and 5 A. Moving to case 3 (600 V and 15 A on xenon), we find that three of the models (Cappelli *et al.*, Chodura, and Data-driven) output discharge currents between 4 and 8 A greater than the experiment while the model of Lafleur *et al.* outputs a discharge current of just 0.5 A lower than the experimental value. Lastly, in case 4 (300 V and 15 A on krypton), both the data-driven model

TABLE IV. Best-fit coefficients for the 300 and 15 A xenon condition, obtained by calibration procedure described in Sec. IV D, compared to values from the literature (cf. Table I).

Model	This work		Literature		
	$c_1$	$c_2$	$c_1$	$c_2$	Reference
Cappelli <i>et al.</i>	1.7	...	0.632	...	18
Chodura	14.5	500.0	1.0	3.0	39
Data-driven	1.295	100.0	2.39	3.32	20
Lafleur <i>et al.</i>	0.057	...	0.102	...	19

22 March 2024 03:08:42

**TABLE V.** Discharge current ( $I_D$ ) predicted by each of the models compared to experimental discharge current.

Case No.	Condition	$I_D$ (experiment, A)	$I_D$ (Cappelli <i>et al.</i> , A)	$I_D$ (Chodura, A)	$I_D$ (data-driven, A)	$I_D$ (Lafleur <i>et al.</i> , A)
1	Xe, 300 V, 15 A	15	14.9	15.2	15.0	14.9
2	Xe, 300 V, 30 A	30	25.6	29.6	27.8	26.5
3	Xe, 600 V, 15 A	15	22.9	18.9	19.3	14.5
4	Kr, 300 V, 15 A	15	14.0	13.3	16.3	10.8

and the model of Cappelli *et al.* show discharge currents, which differ from the measurement by less than 1.5 A. In contrast, the model of Lafleur *et al.* shows a 5 A decrease in discharge current when switching from xenon to krypton propellant, while the Chodura model shows a 3 A increase.

Next, in Table VI, we compare the thrust predicted by the models to the experimental values. In case 1, all four models under-predict the thrust compared to the experiment. The model of Lafleur *et al.* outputs the lowest thrust (77 mN lower than the experimental value), while the Chodura model predicts a thrust of only 7 mN less than the experiment. This discrepancy increases in the 30 A case, where the model with thrust closest to the experiment (the data-driven model) still predicts thrust 100 mN less than the experiment. The agreement with the experiment is improved in case 3, where the data-driven model predicts a thrust value of just 7 mN less than the experimental value. In case 4, the data-driven model again has the best agreement with the experiment, this time over-predicting the thrust by just 3 mN. In all four cases, the model of Lafleur *et al.* has the worst performance of the four models in terms of thrust.

Lastly, in Table VII, we present the integrated velocity residual (IVR) of each of the models at each operating condition. For comparison, we also present the IVR of the empirical reference simulations described in Sec. IV. By design, each of the calibrated empirical reference profiles has IVR less than 0.1, indicating a less than 10% disagreement with the experimental data obtained by LIF across the entire LIF measurement domain. In contrast, the best IVR that any of the models achieves is 0.229 (Chodura model, case 4), but values closer to 0.5 are more typical. As in the thrust results, the model of Lafleur *et al.* has the worst agreement with the spatially resolved ion properties as measured by the integrated velocity residual, with IVRs between 0.67 and 0.79.

There are two major implications of these results. First, while some of these models are able to capture thruster performance and scaling to different operating conditions, none is able to capture all

of these trends. Second, even when a model is able to correctly predict the thruster performance, it may exhibit poor agreement with other data, namely, spatially resolved measurements of plasma properties. Together, these results indicate that these closure models have poor extensibility across thrusters and operating conditions.

To provide insight into the performance of these metrics for the closure models, we present in Fig. 5 the spatially resolved plasma properties from the 300 V and 15 A xenon case extracted along the channel centerline. We note that the results at this operating condition are representative of the other three conditions. In Fig. 5(a), we compare the anomalous collision frequency to the empirically inferred reference profile. We also show the electron cyclotron frequency. The empirical profile exhibits a strong minimum coincident with the location of maximum magnetic field strength (and thus maximum cyclotron frequency). In contrast, the models of Cappelli *et al.* and Chodura show only weak minima, which are displaced half of a discharge channel-length upstream from the minimum of the empirical profile. The anomalous collision frequency predicted by data-driven model does not exhibit a minimum, while the model of Lafleur *et al.* has a steep minimum, albeit shifted half of a channel-length downstream of the thruster exit plane ( $z/L = 1$ ). We return to a discussion of why these predicted anomalous collision frequency profiles differ from the empirical profiles in Sec. VI. Before proceeding with this, however, we examine how these differences in anomalous collision frequency translate to the poor agreement with the experiment.

To this end, in order to explain the variations in the IVR, we show in Fig. 5(b) the axial ion velocity profiles of each of the four models. We compare these results to the LIF data and the ion velocity from the reference simulation. The trends in velocity profiles largely can be explained by the behavior of the collision frequencies in Fig. 5(a). In particular, in Sec. III A, we argued that the peak electric field in the thruster will be coincident with the minimum in anomalous collision frequency and that the

**TABLE VI.** Thrust ( $T$ ) predicted by each of the models compared to experimentally measured thrust.

Case No.	Condition	$T$ (experiment, mN)	$T$ (Cappelli <i>et al.</i> , mN)	$T$ (Chodura, mN)	$T$ (data-driven, mN)	$T$ (Lafleur <i>et al.</i> , mN)
1	Xe, 300 V, 15 A	$292.9 \pm 3.5$	270.3	276.2	258.3	215.5
2	Xe, 300 V, 30 A	$539.0 \pm 4.0$	404.8	473.9	440.4	398.2
3	Xe, 600 V, 15 A	$447.2 \pm 3.0$	400.7	403.9	442.3	273.5
4	Kr, 300 V, 15 A	$235.8 \pm 2.5$	220.7	210.7	238.7	149.0

**TABLE VII.** Integrated velocity residual (IVR) of each of the four models compared to IVR of reference simulation.

Case No.	Condition	IVR (empirical)	IVR (Cappelli <i>et al.</i> )	IVR (Chodura)	IVR (data-driven)	IVR (Lafleur <i>et al.</i> )
1	Xe, 300 V, 15 A	0.069	0.520	0.400	0.417	0.761
2	Xe, 300 V, 30 A	0.095	0.463	0.339	0.393	0.730
3	Xe, 600 V, 15 A	0.065	0.614	0.583	0.538	0.793
4	Kr, 300 V, 15 A	0.059	0.457	0.272	0.347	0.669

magnitude of the electric field should increase as the minimum steepens spatially. With this in mind, given the shallow minima in the models of Chodura and Cappelli *et al.* and the absent minimum in the data-driven model, we would expect these models to produce weaker peak electric fields and thus more gradual ion acceleration than the experimental results. This is indeed the case and can explain the large discrepancy with the experiment. The model of Lafleur *et al.* predicts a steep ion acceleration curve in better qualitative agreement with the experiment than the other three models. This stems directly from the steep and spatially localized minimum in collision frequency. However, since this minimum occurs downstream, so too does the bulk of the ion acceleration, which starts half of a channel-length downstream from the experimental measurements. This consequently results in the largest overall IVR.

We next discuss how variations in the collision frequency profile may contribute to poor predictions in thrust. To this end, we first examine the role of electron temperature. As higher electron temperatures correspond to increased ion production (and therefore thrust), discrepancies in this quantity may serve to explain under/overpredictions in thrust. In this context, we show in Fig. 5(c) the electron temperature extracted along the thruster channel centerline. In terms of peak magnitude in temperature, the data-driven model and the model of Cappelli *et al.* predict peak

electron temperatures of 39 eV, while the Chodura model predicts a peak temperature of 36 eV. The model of Lafleur *et al.* predicts the lowest peak electron temperature, at 33 eV. These results could explain in part why the model of Lafleur *et al.* predicts a lower thrust than the other models. Physically, this may result from the fact that the electron temperature is generally assumed to be isothermal along magnetic field lines in Hall thrusters.<sup>4,12,28</sup> As the magnetic field lines downstream from the thruster exit plane are longer than those closer to the exit plane, the electron thermal energy must therefore be spread out across a larger region of space. A downstream displacement of the anomalous collision frequency profile (as exhibited by the model of Lafleur *et al.* in Fig. 5) and peak electric field could thus shift the location of maximum electron heating in such a way as to reduce the peak electron temperature.

Another explanation for the low predicted thrust of the model of Lafleur *et al.* could be high plume divergence compared to the other models. If all of the ionization and ion acceleration happens far outside of the thruster channel, then the magnetic field is less able to shape and focus the plasma beam. Indeed, it has been shown that displacing the ion acceleration zone in Hall thrusters by a few millimeters downstream can result in an increase in plume divergence and a corresponding reduction in thrust efficiency.<sup>44</sup> To investigate this hypothesis in the context of our results, we present

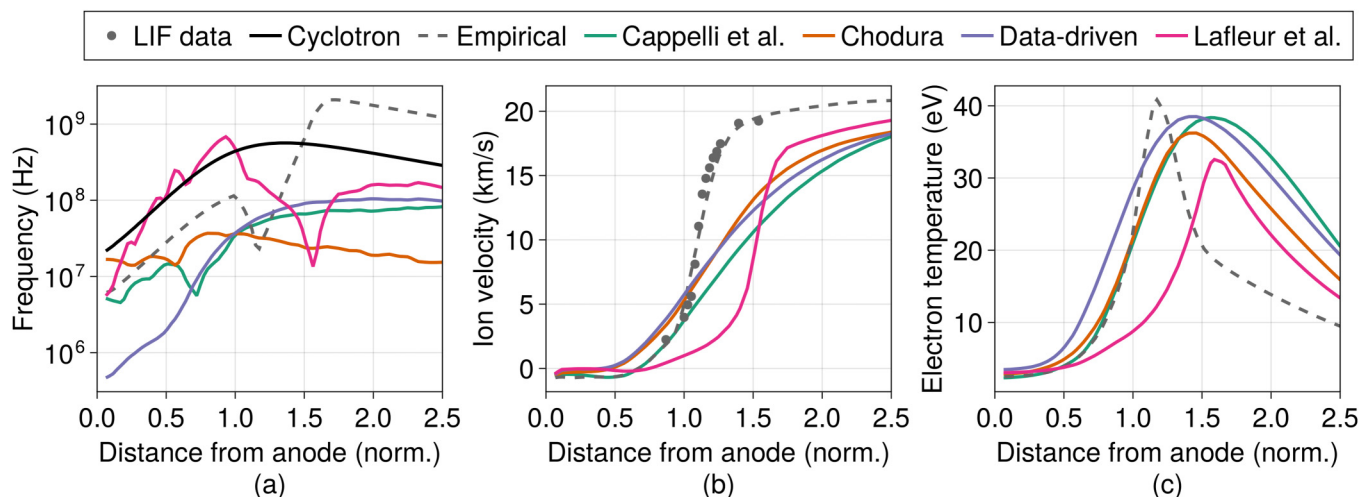


**FIG. 5.** Comparison between model predictions, experimental data, and calibrated reference results of the anomalous collision frequency (a), ion velocity (b), and electron temperature (c) extracted along the channel centerline for case 1 (300 V and 15 A using xenon). All distances are normalized by the length of the discharge channel.

22 March 2024 03:08:42

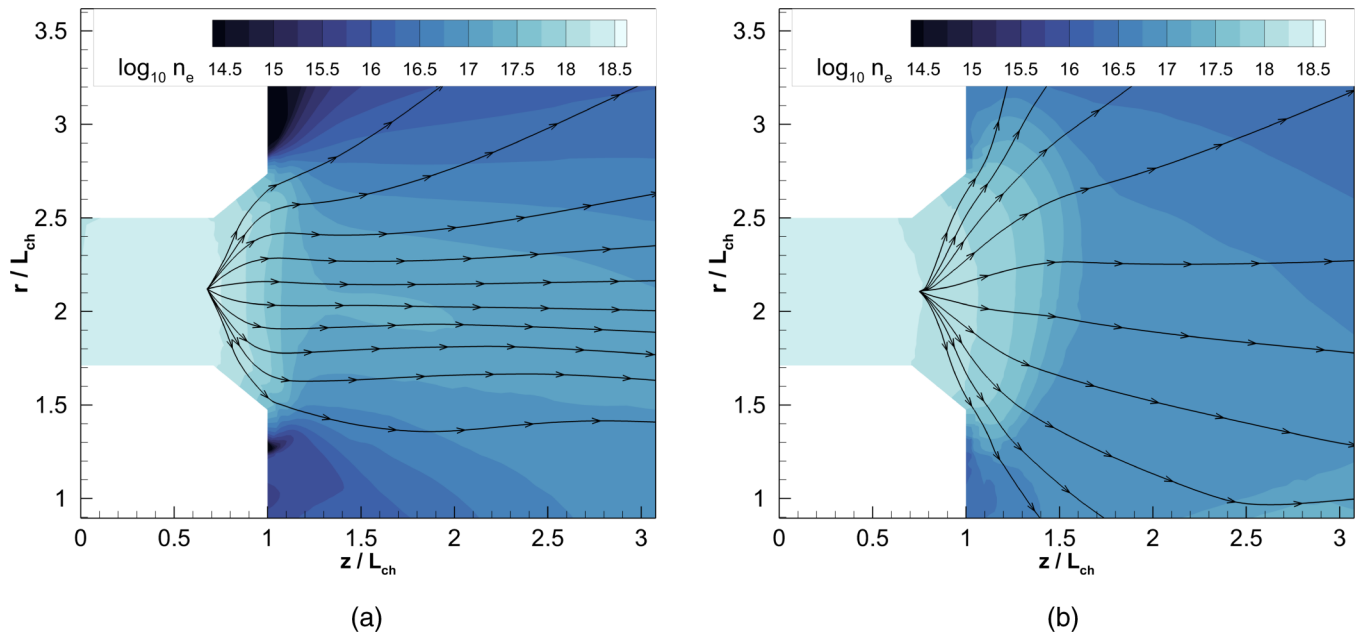


FIG. 6. Ion current density streamlines overlaid on plasma density contours for (a) the calibrated reference simulation and (b) the simulation using the model of Lafleur *et al.* Plasma density is measured in units of  $m^{-3}$  and distances are normalized by the device channel length.

in Fig. 6 a comparison between streamlines of ion current density in the reference case at 300 V and 15 A to the predictions of the model of Lafleur *et al.* As expected, the streamlines are more divergent in this model than in the reference simulation. This means more of the ion momentum is directed in the radial direction and thus unable to contribute to thrust.

In summary, we have shown that none of the investigated models is able to successfully reproduce the experimental measurements, either in terms of global performance metrics or in terms of spatially resolved plasma properties. We can link this behavior to the spatial variation of the anomalous collision frequency as predicted by the four closure models. We turn in Sec. VI to a discussion of the physical processes governing the anomalous collision frequency profiles.

## VI. DISCUSSION

We discuss in this section each model individually. We focus on how the self-consistent coupling of the closure models with the physics of a fluid Hall thruster model like Hall2De may have led to the trends seen in Sec. V. We then highlight the importance of the electron energy balance in this coupling process. Finally, we discuss the implications of this work for informing future closure modeling efforts.

### A. Cappelli *et al.*

As discussed in the original paper<sup>18</sup> and in subsequent work,<sup>20</sup> the model of Cappelli *et al.* may be reduced to the following simpler

expression if the electron pressure gradient is neglected:

$$v_{an} = \omega_{ce} \left( c_1 \frac{v_{de}}{c_e} \right)^2 = \omega_{ce} (c_1 M_e)^2, \tag{17}$$

where  $M_e$  is the azimuthal electron Mach number. In essence, this model predicts that the anomalous collision frequency should follow a Bohm-like scaling, weighted by the square of the electron Mach number. We expect that this scaling should actually produce a peak in the anomalous collision frequency, rather than a minimum, near the peak magnetic field. Per our discussion in Sec. III A, this would lead to poor agreement with experimental measurements.

To illustrate this, we show in Fig. 7 how the electron Mach number along the channel centerline varies with space for the empirical reference simulation for the H9 at 300 V and 15 A. As the magnetic field is a design variable, and the ion velocity and thus electric field are measured to a high degree of accuracy, this can be taken as a relatively accurate picture of what the electron Mach number is in the H9 at this condition. As expected, the electron Mach number peaks sharply just downstream of the thruster exit plane.

We also show the results of applying the model scaling of Eq. (17) to the time-averaged output of the calibrated reference simulation. In doing so, we can assess how the model will react to a reasonable “initial condition” in which the plasma properties closely match experiment. If we apply the model of Cappelli *et al.* to this distribution of plasma properties, we obtain a maximum in the anomalous collision frequency at the precise location where the empirical profile has a minimum. The high transport in this region

22 March 2024 03:08:42

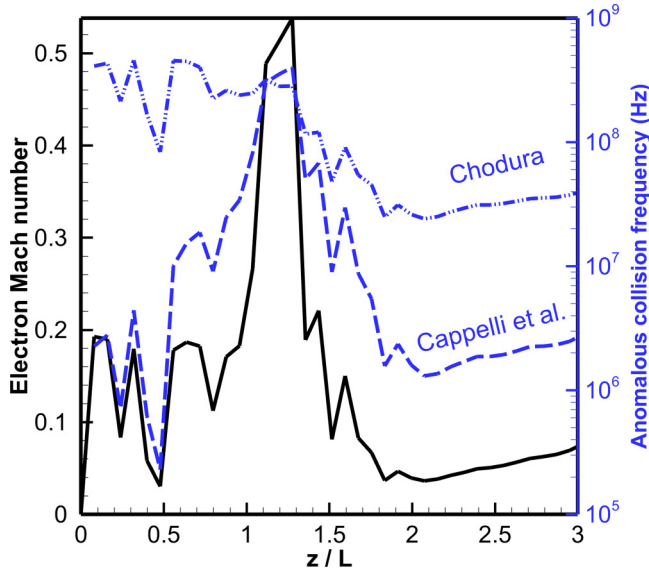


**FIG. 7.** Electron azimuthal Mach number (left axis, black solid line) and evaluated anomalous collision frequencies (right axis) of models of Cappelli *et al.* (blue dashed line) and Chodura (blue dashed-dotted line) along the channel centerline for the calibrated reference simulation at 300 V and 15 A operating on xenon.

would act to reduce the peak electric field, gradually smoothing out the electric field profile and making the ion acceleration profile less steep than experiment. This is what we observed in the preceding section.

### B. Chodura

We can rewrite the Chodura model [Eq. (9)] in terms of the electron Mach number as

$$v_{an} = \omega_{pi} \left[ 1 - \exp\left(-\frac{1}{c_2} \sqrt{\frac{m_i}{m_e}} M_e\right) \right]. \quad (18)$$

In this case, we have a base collision frequency (in this case the ion plasma frequency,  $\omega_{pi}$ ) weighted inversely by a factor which depends on the electron Mach number. In contrast with the model of Cappelli *et al.*, as the Mach number increases, the collision frequency decreases. We, thus, expect intuitively that this model should produce a minimum collision frequency coincident with the peak Mach number (as exhibited by the reference simulation). The conflation factor, however, is that the ion plasma frequency scales with the square root of the plasma density, which in turn decays monotonically with distance from the anode. This makes it difficult to simultaneously obtain the required high degree of transport in the near field plume while also having a minimum near the exit plane. These two factors, thus, compete with each other to produce the collision frequency profile shown in Fig. 7, which is relatively flat over large regions of the domain. Without the strong variations in collision frequency needed to localize the peak electric field, the ions experience gradual, largely constant acceleration.

### C. Data-driven

While we can analyze the behavior of the preceding two models by comparing their behavior to the empirical anomalous collision frequency profile and the plasma properties of the reference simulation, this is not true for the data-driven model, which was developed using exactly these empirical profiles.<sup>20</sup> As shown in the original paper by Jorns<sup>20</sup> and in our recent work,<sup>35</sup> the data-driven model is able to predict the empirical collision frequency profile of the H9 operating at 300 V and 15 A on xenon (case 1) with a high degree of accuracy given only the plasma properties resulting from a simulation run using that empirical profile. This is despite the fact that the H9 was not in its original training dataset.

Instead, we consider how the data-driven model couples with the ion dynamics of the Hall thruster simulation. As the model [Eq. (10)] depends linearly on the ion velocity, the collision frequency should reduce to the classical collision frequency at the ion stagnation point, where  $|\vec{u}_i| = 0$ . As shown in Fig. 2(c), this occurs about 0.7 channel lengths downstream from the anode in the empirical reference simulation. This would recenter the peak electric field (and thus maximum ion acceleration) to this location. The ion stagnation point would then shift further upstream. This process would repeat until the ion stagnation point and minimum collision frequency eventually reach the anode. This explains the nearly monotonic anomalous collision frequency profile seen in Fig. 5(a), and thus the gradual ion acceleration exhibited by this model.

### D. Lafleur *et al.*

While the model of Lafleur *et al.* performed the worst out of the four models in terms of the global performance metrics, it was the only model able to adequately predict the steepness of the ion acceleration profile and the presence of a strong minimum in the anomalous collision frequency. However, the location of this minimum was almost 50% further downstream than the location of the minimum in the empirical profile. One possible reason for this behavior can be motivated from the one-dimensional electron internal energy equation (cf. Ref. 51),

$$\begin{aligned} \frac{\partial}{\partial t} \left( \frac{3}{2} n_e T_e \right) + \frac{\partial}{\partial z} \left( \frac{5}{2} u_{e,z} n_e T_e \right) \\ = m_e n_e v_e |\vec{u}_e|^2 + u_{e,z} \frac{\partial p_e}{\partial z} - S_{loss}. \end{aligned} \quad (19)$$

Here,  $S_{loss}$  represents energy losses to ionization, excitation, and wall effects. Additionally, we have neglected the heat conduction term. We will discuss the effects of this term in Sec. VI E. We make the additional assumption that  $|\vec{u}_e| \approx v_{de}$ . Substituting in the model of Lafleur *et al.* [Eq. (8)], we obtain

$$\begin{aligned} \frac{\partial}{\partial t} \left( \frac{3}{2} n_e T_e \right) + \frac{\partial}{\partial z} \left( \frac{5}{2} u_{e,z} n_e T_e \right) - c_1 M_e \sqrt{\frac{m_i}{m_e}} \frac{\partial}{\partial z} u_{i,z} n_e T_e \\ = m_e n_e v_{e,classical} v_{de}^2 + u_{e,z} \frac{\partial p_e}{\partial z} - S_{loss}. \end{aligned} \quad (20)$$

We note that since  $M_e \sim 0.1$ ,  $c_1 \sim 0.1$ ,  $u_i \sim u_e$ , and  $\sqrt{m_i/m_e} \sim 500$  for xenon, including an anomalous collision frequency of this form introduces an additional convection term to

22 March 2024, 03:08:42

the energy equation with a magnitude comparable to or greater than the original convection term. For the purposes of this discussion, we neglect this term so as to examine the effect of this new convection term in isolation,

$$\begin{aligned} \frac{\partial}{\partial t} \left( \frac{3}{2} n_e T_e \right) - c_1 M_e \sqrt{\frac{m_i}{m_e}} \frac{\partial}{\partial z} u_{i,z} n_e T_e \\ = m_e n_e v_{e, \text{classical}} v_{de}^2 + u_{e,z} \frac{\partial p_e}{\partial z} - S_{\text{loss}}. \end{aligned} \quad (21)$$

The dynamics of this modified energy equation are significantly different from the original equation [Eq. (19)]. The most salient difference is that the electron thermal energy now convects with the ion drift speed instead of the axial electron velocity. In a typical one-dimensional Hall thruster discharge, the axial electron velocity is significantly reduced near the location of peak magnetic field and low anomalous transport [cf. Eq. (4)]. This, combined with the strong Joule heating at this location, has the effect of localizing the electron temperature profile to this point. In the modified energy equation [Eq. (21)], both of these localizing factors are diminished. As the heating rate now scales with  $v_{e, \text{classical}}$  instead of  $v_e$ , the impact of Joule heating on the energy balance is reduced by at least an order of magnitude. Additionally, the axial ion velocity in a Hall thruster increases monotonically moving downstream of the anode, with no minima which would anchor the new convection term. Taken together, these factors explain how the electron temperature profile (and thus the anomalous collision frequency profile, which depends self-consistently on the electron temperature) is displaced so far downstream in the model of Lafleur *et al.* compared to the reference simulation. The magnitude of this displacement would then be determined by the balance between the convection term and the other source terms. This suggests that loss terms which are captured under  $S_{\text{loss}}$  may be more important in determining the one-dimensional structure of the plasma when using anomalous transport models which depend self-consistently on the convection of electron thermal energy.

The absolute value in Eq. (21) adds an additional degree of complexity to our interpretation, as its appearance in the energy transport equation is not exactly the same as a typical convection term. We could more conventionally interpret this term as representing enhanced heating due to anomalous scattering processes. We note that since this heating rate scales in part with the ion velocity, which increases monotonically moving downstream along the channel centerline, the anomalous term may bias the electron heating rate in such a way that the peak in electron pressure occurs further downstream than in the reference simulation. This would then shift the anomalous collision frequency and ion velocity curves in the same manner outlined in the above paragraphs.

The other challenge we encountered with the model of Lafleur *et al.* was its poor performance on case 4 (krypton at 300 V and 15 A). The predicted discharge current was 40% lower than the experimental value, indicating that the anomalous transport is lower than it should be at this operating condition. This suggests that the model may not properly capture the species-dependence of the instability-driven transport.

## E. Role of electron heat flux

Aside from the discrepancies with the experiment already discussed, one feature common to all of the models investigated in this work, including the multi-zone Bohm reference profile, is broad electron temperature profiles. In Fig. 5(c), we see that the predicted electron temperatures two channel-lengths downstream of the exit plane are on the order of 10–20 eV. Experimental measurements of the temperature in this region suggest that these values are too high, with the true temperature likely being between 3 and 7 eV.<sup>30,52</sup> This phenomenon has been observed in other Hall thruster simulation works,<sup>53</sup> and it has been remarked<sup>26</sup> that it is difficult to simultaneously match the experimental electron temperature and ion velocity measurements using an empirically calibrated multi-zone anomalous collision frequency profile.

One factor that may explain this is the electron heat conduction, which we have neglected to this point. In Hall2De, as in other Hall thruster models,<sup>46</sup> the conductive heat flux is assumed to follow Fourier's law of conduction:

$$\vec{q}_e = \kappa_e \nabla T_e, \quad (22)$$

where  $\vec{q}_e$  is the electron heat flux vector and  $\kappa_e$  is the anisotropic electron thermal conductivity tensor. The cross-field component of this tensor is given by Ref. 54,

$$\kappa_{\perp, e} = 4.7 \frac{v_e n_e T_e}{m_e \omega_{ce}^2}. \quad (23)$$

This expression is derived under the assumption that the heat conduction is moderated by classical electron-ion collisions, i.e.,  $v_e = v_{ei}$ . In Hall2De, in order to approximate the effect of the anomalous transport on the heat flux, we use the sum of anomalous and classical collision frequencies in this expression, i.e.,  $v_e \approx v_{ei} + v_{an}$  as we do for the generalized Ohm's law [Eq. (4)]. This is common in other models of low-temperature plasmas in electric propulsion.<sup>46,51</sup> However, the theoretical underpinnings of this substitution are suspect. While it can be shown that many of the proposed mechanisms that contribute to anomalous electron momentum transport can be approximated using an effective collision frequency in a generalized Ohm's law, there has yet to be a demonstration that the classical Fourier law can be modified in a similar way. Indeed, the Fourier law is valid under the assumption that the collisions serve to relax the electron velocity distribution function back to equilibrium, while the processes that produce the anomalous "collisions" may not have the same effect. For example, if the transport is driven by the growth and convection of plasma waves, the thermal transport may be affected in a more complex manner which cannot be easily represented in a Fourier-like formulation.

The fact that the electron temperature profiles are too wide indicates that incorporating the anomalous collision frequency into Eq. (23) may lead to an over-estimate of the true cross-field thermal conductivity. Accurate modeling of the effect of anomalous processes on the electron heat flux, as well as the impacts of other non-ideal and anisotropic processes in the electron energy balance,<sup>55</sup> may be important to fully capture the effect of anomalous electron transport on Hall thruster discharge plasmas.

22 March 2024 03:08:42

## F. Implications for closure model development

In the present work, we have focused on time-averaged or steady simulation results for evaluating the efficacy of the chosen closure models. The time-resolved thruster behavior may be another important and critical metric for comparison. This stems from the fact that Hall thrusters can exhibit large-scale oscillations in internal plasma properties,<sup>30</sup> including the anomalous collision frequency. We have discussed the role of the transient behavior of the thruster with respect to evaluating closure models in more detail in Ref. 35.

In that work, we also showed that the ability of an anomalous collision frequency model to reproduce measured electron transport profiles when evaluated with time-averaged or steady plasma data does not guarantee the closure model will perform well when implemented directly into a Hall thruster simulation. We theorized that the strong coupling between the anomalous transport model and the Hall thruster model can cause the simulation to quickly diverge to a new equilibrium profile. This is supported by the present work, in which we found that the behavior of all four models can be explained by considering the feedback between the anomalous collision frequency model and the fluid Hall thruster model. With these results in mind, our findings recommend some guidance for refining new closure models of the Hall thruster anomalous electron transport.

First, as suggested by our previous work, it is not sufficient to evaluate a model of the anomalous collision frequency against time-averaged plasma data, whether experimental or numerical. To evaluate the predictive ability of a closure model, it must be implemented directly into a Hall thruster code, and the collision frequency must be allowed to vary self-consistently with the plasma properties it depends on.

Second, as highlighted by the results of the model of Lafleur *et al.* and our subsequent discussion of the electron heat flux, the electron energy balance appears to play a critical role in the coupling between the functional form of the closure model and the rest of the Hall thruster model. When developing a new closure model for the anomalous collision frequency, it is thus important to consider the effect of the model not just on the momentum balance but also on the energy balance.

Lastly, it is critical that proposed models must be tested against multiple operating conditions, and ideally, multiple thrusters. Extensibility with voltage, current, propellant choice, magnetic field strength, thruster geometry, and background pressure should be considered. Particular emphasis should be placed on matching spatially resolved plasma properties in addition to targeting the global performance metrics.

## VII. CONCLUSION

In this work, we have assessed the predictive capabilities of closure models for the anomalous electron transport in Hall effect thrusters. We implemented these models self-consistently into Hall2De, a PIC/multi-fluid Hall thruster code developed by the Jet Propulsion Laboratory, and compared their performance on four operating conditions of the H9 Hall thruster to experimental data obtained at the University of Michigan. We investigated four models. The first was based on classical turbulence theory, the

second on empirical scaling laws, the third on the scaling of the electron drift instability in Hall thrusters, and the last from data. We calibrated the coefficients of these models to match the experimental discharge current of one of these four conditions and then applied these calibrated coefficients to the other three operating conditions. In this way, we were able to assess the ability of the models to generalize across operating conditions. To our knowledge, this is the first comprehensive comparison of different models of anomalous electron transport using the same simulation code and operating conditions.

While a few of the models were able to capture some of the scaling trends with discharge current and changes in propellant, most exhibited incorrect scaling of thrust and discharge current with increasing discharge voltage. Additionally, three of the models exhibited relaxed ion acceleration profiles and were unable to capture the strong reduction in anomalous transport coincident with the location of the maximum radial magnetic field. In the model based on the electron drift instability, the observed ion acceleration curves were more in line with experimental data, but the location of the acceleration zone was shifted downstream by half of a channel length.

We then explained the performance of each of the models by considering the coupling between the closure models and the simulation dynamics. In all four cases, we showed that the dependence of these models on local plasma properties will drive the converged solution away from the experimental data. Thus, even though these models are predicated on physics-based hypotheses or derived directly from data, their functional scalings are evidently incorrect. Relatedly, one common element to all of the models, even those calibrated to match data, is that they predict electron temperature profiles more relaxed than the experiments suggest. While this can be attributed partially to the form of the collision frequency in each of the models, it may also result from an over-simplification of how anomalous momentum transport impacts anomalous heat conduction. With that said, the insights we have gained from analyzing the limitations of these models suggest some guidelines for future efforts to develop a predictive model of anomalous electron transport in Hall thrusters.

## ACKNOWLEDGMENTS

The authors would like to acknowledge Dr. Ioannis Mikellides and Dr. Alejandro Lopez Ortega at the Jet Propulsion Laboratory for allowing us to use and modify Hall2De. We would also like to acknowledge Ms. Leanne L. Su for her work in calibrating reference simulations of the H9 Hall thruster using Hall2De in addition to copyediting, as well as fruitful discussions with Professor Mark Cappelli via email. We also acknowledge Mr. Parker J. Roberts and Mr. Declan G. Brick for assistance in editing this manuscript. This research was supported in part through computational resources and services provided by Advanced Research Computing at the University of Michigan, Ann Arbor, and was funded in part by the Strategic Research Institute and Joint Advanced Propulsion Institute of the National Aeronautics and Space Administration, and by United States Air Force Office of Scientific Research (Grant No. FA9550-19-1-002) through the Space Propulsion and Power Program Portfolio.

22 March 2024 03:08:42

## AUTHOR DECLARATIONS

## Conflict of Interest

The authors have no conflicts to disclose.

## Author Contributions

**Thomas A. Marks:** Conceptualization (equal); Data curation (equal); Formal analysis (equal); Investigation (equal); Methodology (equal); Software (equal); Visualization (equal); Writing – original draft (equal); Writing – review & editing (equal). **Benjamin A. Jorns:** Conceptualization (equal); Funding acquisition (equal); Project administration (equal); Resources (equal); Supervision (equal); Writing – review & editing (equal).

## DATA AVAILABILITY

The data that support the findings of this study are available from the corresponding author upon reasonable request.

## REFERENCES

- <sup>1</sup>J. Jackson, M. Allen, R. Myers, E. Soendker, B. Welander, A. Tolentino, S. Hablitzel, C. Yeatts, C. Sheehan, J. Cardin, J. S. Snyder, R. R. Hofer, T. Tofil, and D. Herman, “13 kW advanced electric propulsion flight system development and qualification,” in *The 36th International Electric Propulsion Conference* (Electric Rocket Propulsion Society, 2019), p. 18.
- <sup>2</sup>J. S. Snyder, D. M. Goebel, V. Chaplin, A. L. Ortega, I. G. Mikellides, F. Aghazadeh, I. Johnson, T. Kerl, and G. Lenguito, “Electric propulsion for the Psyche mission,” in *36th International Electric Propulsion Conference* (Electric Rocket Propulsion Society, 2019).
- <sup>3</sup>J. S. Snyder, V. Chaplin, D. M. Goebel, R. R. Hofer, A. L. Ortega, I. G. Mikellides, T. Kerl, G. Lenguito, F. Aghazadeh, and I. Johnson, “Electric propulsion for the Psyche mission: Development activities and status,” in *AIAA Propulsion and Energy 2020 Forum* (AIAA, 2020), pp. 1–15.
- <sup>4</sup>J. P. Boeuf, “Tutorial: Physics and modeling of Hall thrusters,” *J. Appl. Phys.* **121**, 011101 (2017).
- <sup>5</sup>I. G. Mikellides, I. Katz, R. R. Hofer, and D. M. Goebel, “Magnetic shielding of a laboratory Hall thruster. I. Theory and validation,” *J. Appl. Phys.* **115**, 043303 (2014).
- <sup>6</sup>J. Brophy, J. Polk, and J. Dankanich, “Lifetime qualification standard for electric thrusters,” in *45th AIAA/ASME/SAE/ASEE Joint Propulsion Conference & Exhibit* (AIAA, 2009).
- <sup>7</sup>J. Cavalier, N. Lemoine, G. Bonhomme, S. Tsikata, C. Honoré, and D. Grésillon, “Hall thruster plasma fluctuations identified as the e-b electron drift instability: Modeling and fitting on experimental data,” *Phys. Plasmas* **20**, 082107 (2013).
- <sup>8</sup>B. Vincent, S. Tsikata, S. Mazouffre, T. Minea, and J. Fils, “A compact new incoherent Thomson scattering diagnostic for low-temperature plasma studies,” *Plasma Sources Sci. Technol.* **27**, 055002 (2018).
- <sup>9</sup>D. L. Brown, C. W. Larson, B. E. Beal, and A. D. Gallimore, “Methodology and historical perspective of a Hall thruster efficiency analysis,” *J. Propul. Power* **25**, 31 (2020).
- <sup>10</sup>W. Villafana, B. Cuenot, and O. Vermorel, “3D particle-in-cell study of the electron drift instability in a Hall thruster using unstructured grids,” *Phys. Plasmas* **30**, 033503 (2023).
- <sup>11</sup>M. Reza, F. Faraji, A. Knoll, A. Piragino, T. Andreussi, and T. Misuri, “Reduced-order particle-in-cell simulations of a high-power magnetically shielded Hall thruster,” *Plasma Sources Sci. Technol.* **32**, 065016 (2023).
- <sup>12</sup>I. G. Mikellides and I. Katz, “Numerical simulations of Hall-effect plasma accelerators on a magnetic-field-aligned mesh,” *Phys. Rev. E* **86**, 046703 (2012).
- <sup>13</sup>R. R. Hofer, H. Kamhawi, D. A. Herman, J. E. Polk, J. S. Snyder, I. G. Mikellides, W. Huang, J. L. Myers, J. T. Yim, G. J. Williams, A. L. Ortega,

B. A. Jorns, M. J. Sekerak, C. Griffith, R. Shastry, T. W. Haag, T. Verhey, B. Gilliam, I. Katz, D. M. Goebel, J. R. Anderson, J. H. Gilland, and L. Clayman, “Development approach and status of the 12.5 kW HERMeS Hall thruster for the solar electric propulsion technology demonstration mission,” in *34th International Electric Propulsion Conference* (Electric Rocket Propulsion Society, 2015).

<sup>14</sup>I. G. Mikellides and A. L. Ortega, “2D (r–z) numerical simulations of the plasma and channel erosion in a 100 kW class nested Hall thruster,” *Plasma Sources Sci. Technol.* **27**, 075001 (2018).

<sup>15</sup>C. M. Lam, E. Fernandez, and M. A. Cappelli, “A 2D hybrid Hall thruster simulation that resolves the  $E \times B$  electron drift direction,” *IEEE Trans. Plasma Sci.* **43**, 86–94 (2015).

<sup>16</sup>R. Kawashima and K. Komurasaki, “Two-dimensional hybrid model of gradient drift instability and enhanced electron transport in a Hall thruster,” *Phys. Plasmas* **28**, 063502 (2021).

<sup>17</sup>M. K. Scharfe, C. A. Thomas, D. B. Scharfe, N. Gascon, M. A. Cappelli, and E. Fernandez, “Shear-based model for electron transport in hybrid Hall thruster simulations,” *IEEE Trans. Plasma Sci.* **36**, 2058–2068 (2008).

<sup>18</sup>M. A. Cappelli, C. V. Young, E. Cha, and E. Fernandez, “A zero-equation turbulence model for two-dimensional hybrid Hall thruster simulations,” *Phys. Plasmas* **22**, 114505 (2015).

<sup>19</sup>T. Lafleur, S. D. Baalrud, and P. Chabert, “Theory for the anomalous electron transport in Hall effect thrusters. I. Insights from particle-in-cell simulations,” *Phys. Plasmas* **23**, 053502 (2016).

<sup>20</sup>B. Jorns, “Predictive, data-driven model for the anomalous electron collision frequency in a Hall effect thruster,” *Plasma Sources Sci. Technol.* **27**, 104007 (2018).

<sup>21</sup>G. Alfonsi, “Reynolds-averaged Navier–Stokes equations for turbulence modeling,” *Appl. Mech. Rev.* **62**, 040802 (2009).

<sup>22</sup>I. Katz, A. L. Ortega, B. A. Jorns, and I. G. Mikellides, Growth and saturation of ion acoustic waves in Hall thrusters,” in *2016 AIAA Propulsion and Energy Forum* (AIAA, 2016).

<sup>23</sup>B. A. Jorns, “Two equation closure model for plasma turbulence in a Hall effect thruster,” in *36th International Electric Propulsion Conference* (Electric Rocket Propulsion Society, 2019), pp. 1–12.

<sup>24</sup>M. K. Scharfe, N. Gascon, M. A. Cappelli, and E. Fernandez, “Comparison of hybrid Hall thruster model to experimental measurements,” *Phys. Plasmas* **13**, 083505 (2006).

<sup>25</sup>J. W. Koo and I. D. Boyd, “Modeling of anomalous electron mobility in Hall thrusters,” *Phys. Plasmas* **13**, 3541 (2006).

<sup>26</sup>I. G. Mikellides and A. L. Ortega, “Challenges in the development and verification of first-principles models in Hall-effect thruster simulations that are based on anomalous resistivity and generalized Ohm’s law,” *Plasma Sources Sci. Technol.* **28**, 014003 (2019).

<sup>27</sup>R. Hofer, I. Mikellides, I. Katz, and D. Goebel, “Wall sheath and electron mobility modeling in hybrid-PIC Hall thruster simulations,” in *43rd AIAA/ASME/SAE/ASEE Joint Propulsion Conference & Exhibit* (AIAA, 2007), <https://arc.aiaa.org/doi/pdf/10.2514/6.2007-5267>.

<sup>28</sup>D. M. Goebel and I. Katz, *Fundamentals of Electric Propulsion: Ion and Hall Thrusters* (Jet Propulsion Laboratory, 2008).

<sup>29</sup>R. Hofer, I. Katz, D. Goebel, K. Jameson, R. Sullivan, L. Johnson, and I. Mikellides, “Efficacy of electron mobility models in hybrid-PIC Hall thruster simulations,” in *44th AIAA/ASME/SAE/ASEE Joint Propulsion Conference & Exhibit* (AIAA, 2012).

<sup>30</sup>E. T. Dale and B. A. Jorns, “Non-invasive time-resolved measurements of anomalous collision frequency in a Hall thruster,” *Phys. Plasmas* **26**, 013516 (2019).

<sup>31</sup>S. Tsikata, N. Lemoine, V. Pisarev, and D. M. Grésillon, “Dispersion relations of electron density fluctuations in a Hall thruster plasma, observed by collective light scattering,” *Phys. Plasmas* **16**, 33506 (2009).

<sup>32</sup>S. Tsikata, A. Héron, and C. Honoré, “Hall thruster microturbulence under conditions of modified electron wall emission,” *Phys. Plasmas* **24**, 053519 (2017).

<sup>33</sup>Z. A. Brown and B. A. Jorns, “Spatial evolution of small wavelength fluctuations in a Hall thruster,” *Phys. Plasmas* **26**, 113504 (2019).



- <sup>34</sup>Z. A. Brown and B. A. Jorns, "Growth and saturation of the electron drift instability in a crossed field plasma," *Phys. Rev. Lett.* **130**, 115101 (2023).
- <sup>35</sup>T. A. Marks and B. A. Jorns, "Challenges with the self-consistent implementation of closure models for anomalous electron transport in fluid simulations of Hall thrusters," *Plasma Sources Sci. Technol.* **32**, 045016 (2023).
- <sup>36</sup>R. Chodura, G. Bardotti, and F. Engelmann, "Numerical investigation of the anomalous resistivity due to two-stream instability," *Plasma Phys.* **13**, 1099 (1971).
- <sup>37</sup>D. Biskamp and R. Chodura, "Computer simulation of anomalous DC resistivity," *Phys. Rev. Lett.* **27**, 1553–1556 (1971).
- <sup>38</sup>A. G. Sgro and C. W. Nielson, "Hybrid model studies of ion dynamics and magnetic field diffusion during pinch implosions," *Phys. Fluids* **19**, 126–133 (1976).
- <sup>39</sup>R. D. Milroy and J. U. Brackbill, "Numerical studies of a field-reversed theta-pinch plasma," *Phys. Fluids* **25**, 775–783 (1982).
- <sup>40</sup>M. E. Kayama, "Resistivity in the dynamic current sheath of a field reversed configuration," *Phys. Plasmas* **19**, 032511 (2012).
- <sup>41</sup>J. Simmonds, Y. Raitses, and A. Smolyakov, "A theoretical thrust density limit for Hall thrusters," *J. Electr. Propul.* **2**, 12 (2023).
- <sup>42</sup>R. R. Hofer, S. E. Cusson, R. B. Lobbia, and A. D. Gallimore, "The H9 magnetically shielded Hall thruster" in *35th International Electric Propulsion Conference* (2017).
- <sup>43</sup>S. E. Cusson, R. R. Hofer, R. B. Lobbia, B. A. Jorns, and A. D. Gallimore, "Performance of the H9 magnetically shielded Hall thrusters," in *35th International Electric Propulsion Conference* (Electric Rocket Propulsion Society, 2017).
- <sup>44</sup>L. L. Su and B. A. Jorns, "Performance comparison of a 9-kW magnetically shielded Hall thruster operating on xenon and krypton," *J. Appl. Phys.* **130**, 163306 (2021).
- <sup>45</sup>L. L. Su and B. Jorns, "Performance at high current densities of a magnetically-shielded Hall thruster," in *AIAA Propulsion and Energy 2021 Forum* (AIAA, 2021).
- <sup>46</sup>J. M. Fife, "Hybrid-PIC modeling and electrostatic probe survey of Hall thrusters," Ph.D. thesis (Massachusetts Institute of Technology, 1998).
- <sup>47</sup>J. Perales-Díaz, A. Domínguez-Vázquez, P. Fajardo, E. Ahedo, F. Faraji, M. Reza, and T. Andreussi, "Hybrid plasma simulations of a magnetically shielded Hall thruster," *J. Appl. Phys.* **131**, 103302 (2022).
- <sup>48</sup>M. P. Georgin, B. A. Jorns, and A. D. Gallimore, "Transient non-classical transport in the hollow cathode plume I: Measurements of time-varying electron collision frequency," *Plasma Sources Sci. Technol.* **29**, 105010 (2020).
- <sup>49</sup>T. Marks, P. Schedler, and B. Jorns, "Hallthruster.jl: A julia package for 1D Hall thruster discharge simulation," *J. Open Source Software* **8**, 4672 (2023).
- <sup>50</sup>T. A. Marks and B. A. Jorns, "Modeling anomalous electron transport in Hall thrusters using surrogate methods," in *37th International Electric Propulsion Conference* (Electric Rocket Propulsion Society, 2022).
- <sup>51</sup>K. Hara, "Non-oscillatory quasineutral fluid model of cross-field discharge plasmas," *Phys. Plasmas* **25**, 123508 (2018).
- <sup>52</sup>E. Dale, "Investigation of the Hall thruster breathing mode," Ph. D thesis, University of Michigan (2019).
- <sup>53</sup>A. L. Ortega, B. Jorns, I. G. Mikellides, and R. R. Hofer, "Numerical simulations of the XR-5 Hall thruster for life assessment at different operating conditions," in *51st AIAA/SAE/ASEE Joint Propulsion Conference* (AIAA, 2015), <https://arc.aiaa.org/doi/pdf/10.2514/6.2015-4008>.
- <sup>54</sup>S. I. Braginskii, "Transport processes in a plasma," *RvPP* **1**, 205 (1965); available at [https://static.ias.edu/pitp/2016/sites/pitp/files/braginskii\\_1965-1.pdf](https://static.ias.edu/pitp/2016/sites/pitp/files/braginskii_1965-1.pdf)
- <sup>55</sup>Y. Yamashita, R. Lau, and K. Hara, "Inertial and anisotropic pressure effects on cross-field electron transport in low-temperature magnetized plasmas," *J. Phys. D: Appl. Phys.* **56**, 384003 (2023).